Ultrahigh-temperature osumilite gneisses in southern Madagascar record combined heat advection and high rates of radiogenic heat production in a long-lived high-temperature orogen

Robert M. Holder, Bradley R. Hacker, Forrest Horton, and A. F. Michel Rakotondrazafy

APPENDIX S1: FINITE-DIFFERENCE RADIOGENIC-HEAT-PRODUCTION & LITHOSPHERIC-HEAT-CONDUCTION MODELS

Here we outline the details of the models used to generate the thermal gradients shown in figure 11a. For the crust, the heat capacity and thermal diffusivity were temperature dependent, following the expressions of Whittington, Hofmeister, and Nabelek (2009). The crustal heat capacity was further modified to account for the latent heat of crystallization following the parameterization of Stüwe (1995). The solidus and liquidus were 750 and 1050 °C for the upper crust, 800 and 1100 °C for the middle crust, and 850 and 1150 °C for the lower crust. The latent heat of crystallization was 320 J/g as recommended by Stüwe (1995). The fraction of melt was assumed to increase linearly between the solidus and liquidus. Melt transfer was not modeled. Mantle heat capacity and thermal diffusivity were temperature and pressure dependent according the parameterization of Xu et al. (2004). Partial melting was not modeled in the mantle. The density of the crust was 2700 kg/m^3 and the mantle was 3300 kg/m^3. Temperature at the surface was fixed at 0 °C and the base of the mantle lithosphere was 1300 °C. Model resolutions were 250 m and 1.6875 x 10^{10} s. The models began with a 30 km thick crust with an equilibrium thermal gradient. The crust was then instantly thickened to 60 km by pure shear (new nodes were inserted at every other depth step within the crust and the temperature at these new nodes was interpolated from the adjacent nodes) and the geothermal gradient was allowed to relax for 100 Ma. The thermal gradients in Figure 12a are for t = 40 Ma: slightly longer than the maximum duration of heating permissible by monazite geochronology (< 29 ± 8 Ma, see section 5.1.2 of main text).

Models using three different high-heat-production-rate profiles are presented: 1) a model with a homogenous heat-production rate of 2 µW/m³, 2) a model with a homogeneous heat-production rate of 3 µW/m³, and 3) a model using the average heat production profile of southeastern Madagascar from Horton, Hacker, Kylander-Clark, Holder, and Jöns (2016). Each of these models has a middle- to lower-crustal heat-production rate > 3x the heat-production rate estimated for average cratons (Hacker, Kelemen, & Behn, 2011; Rudnick & Gao, 2013). The homogeneous 3 µW/m³ model and the Horton et al. model have middle-to-lower crustal heat-production rates slightly higher than average granite (2.4 µW/m³) thus providing a maximum plausible heat-production rate for large portions of the crust.

APPENDIX S2: EMPLACEMENT TEMPERATURES OF THE ANOSYEN BATHOLITH

To further investigate the role of heat advected during emplacement of the Anosyen Batholith, the emplacement temperatures of orthopyroxene-bearing granites and syenites were calculated by determining the fraction of melt as a function of temperature with the program rhyoliteMELTS (Gualda, Ghiorso, Lemons, & Carley, 2012). Seven bulk-rock compositions reported by GAF-BGR (2008) were modeled; these compositions and their corresponding sample numbers are shown in Table S8. They were modeled as anhydrous because of the dearth or absence of primary hydrous phases in these rocks (Paquette et al. 1994; GAF-BGR 2008). Calculations were made assuming a pressure of 0.6 GPa. Figure S2 shows the wt.% melt for each whole-rock composition as a function of temperature.

APPENDIX S3: REFENCE MATERIALS & REDUCTION OF LASS MONAZITE & ZIRCON DATA

Bananeira monazite was used as the primary reference material for monazite (Kylander-Clark, Hacker, & Cottle, 2013; Palin et al., 2013), because it returned the most homogeneous uncorrected values throughout all runs. Monazite 44069, Moacyr, FC-1, Trebilcock, and Manangotry monazites were run as secondary reference materials (Aleinikoff et al., 2006; de Oliveira Gonçalves et al., 2015; Horstwood, Foster, Parrish, Noble, & Nowell, 2003; Tomascak, Krogstad, & Walker, 1996). All monazite dates reported in this study are corrected by a factor of -1.0 ± 0.2 %, based on the weighted mean offset between the LA-ICP-MS data and the reported TIMS values of the secondary reference materials FC-1, Moacyr, and 44069. Zircon 91500 (Wiedenbeck et al., 1995) was used as the primary reference material for U–Pb isotope ratios. GJ-1 zircon (Jackson, Pearson, Griffin, & Belousova, 2004) was used a secondary reference material for U–Pb analyses and the primary reference material for trace-element analyses. Plešovice zircon (Sláma et al., 2008) was used an as additional secondary reference material.

   Monazite compositions measured by Agilent 7700x quadrupole ICP-MS were initially reduced assuming 12 wt. % P as an internal standard and then normalized to 100 wt. % total oxides of all measured elements. Monazite compositions measured by Nu AttoM ICP-MS included only lanthanide concentrations; data were reduced assuming Pr ppm = 29,000 (the average value returned by the former method). The logic behind this decision was that Pr concentrations vary the least among the measured lanthanides in the samples reduced by the former method.

   In zircon, trace elements other than Ti were reduced assuming stoichiometric Zr in $ZrSiO_4$ as an internal standard. Ti concentrations were reduced by creating a calibration line of Ti counts per second vs. Ti concentration for GJ-1 and 91500 zircons; the calibration line was anchored to the origin. The zircon in this study had Ti concentrations 5–10 times greater than the reference materials; 2σ uncertainty in the calibration line was propagated into each unknown Ti concentration. Ti-in-zircon temperatures were calculated using the experimental calibration of Ferry and Watson (2007) with P = 0.6 ± 0.1 GPa and $a_{TiO2} = 0.75 \pm 0.25$ (rutile is not present); the 2σ uncertainty in the Ti concentrations and the experimental calibration coefficients were also propagated into the calculated temperatures. Individual Ti-in-zircon temperatures have an accuracy of ± 60 °C (2σ).

Figure S1. Monazite from a leucocratic segregation in sample 23A has oscillatory Th zoning and is nearly homogeneous in Y. This monazite is interpreted to have formed from crystallization of partial melt and thus provide a minimum date for the peak temperature of metamorphism. All analyses are 550 ± 6 Ma (Figure 7g).
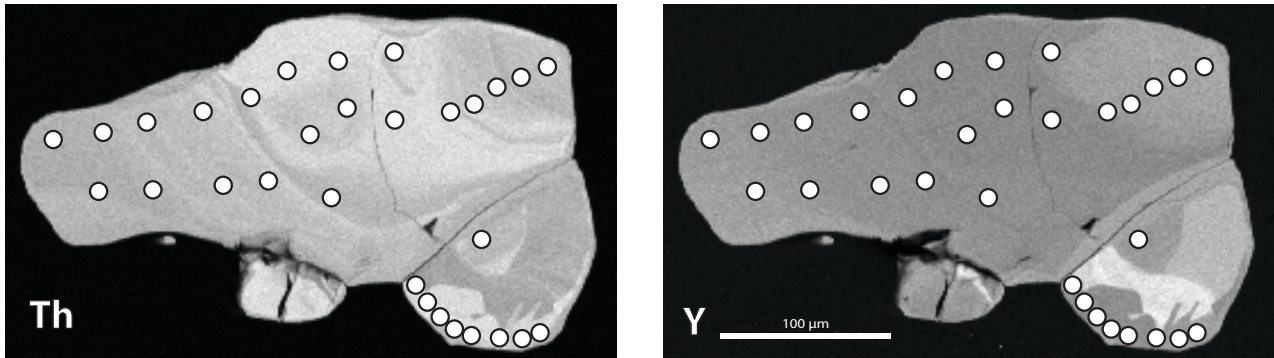
monazite from leucocratic segregation in sample 23A.
U–Pb date (all analyses) = 550 ± 6 Ma, MSWD = 1.1, n = 31 (Fig. 7g)

Figure S2. Weight fraction silicate melt as a function of temperature for seven orthopyroxene-bearing granitoids from the Anosyen Batholith. The granitoids were likely emplaced at temperatures > 1000 °C, suggesting that they may have been an important heat source for metamorphism of the surrounding gneisses, which reached temperatures of 900–950 °C. See Appendix S2 for more information.
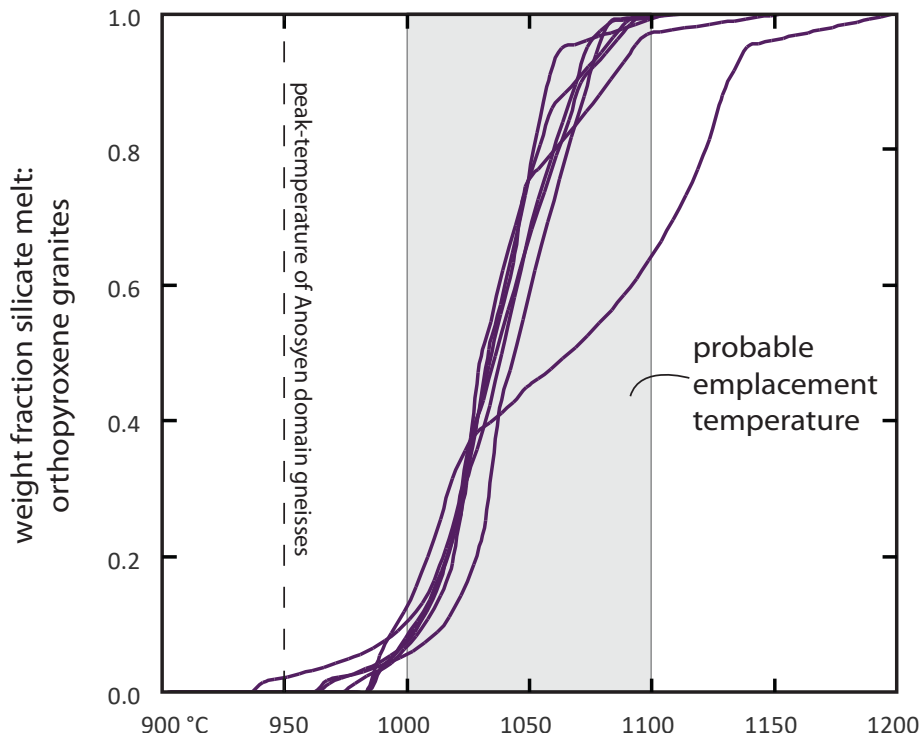
REFERENCES

Aleinikoff, J. N., Schenck, W. S., Plank, M. O., Srogi, L. A., Fanning, C. M., Kamo, S. L., & Bosbyshell, H. (2006). Deciphering igneous and metamorphic events in high-grade rocks of the Wilmington complex, Delaware: Morphology, cathodoluminescence and backscattered electron zoning, and SHRIMP U-Pb geochronology of zircon and monazite. Bulletin of the Geological Society of America, 118(1–2), 39–64. https://doi.org/10.1130/B25659.1

Goncalves, G. O., Lana, C., Scholz, R., Buick, I. S., Gerdes, A., Kamo, S. L., . . . Nalini, H. A. (2016). An assessment of monazite from the Itambe pegmatite district for use as U-Pb isotope reference material for microanalysis and implications for the origin of the "Moacyr" monazite. Chemical Geology, 424(2016), 30–50. https://doi.org/10.1016/j.chemgeo.2015.12.019

Hacker, B. R., Kelemen, P. B., & Behn, M. D. (2011). Differentiation of the continental crust by relamination. Earth and Planetary Science Letters, 307, 501–516. https://doi.org/10.1016/j.epsl.2011.05.024

Horstwood, M. S. A., Foster, G. L., Parrish, R. R., Noble, S. R., & Nowell, G. M. (2003). Common-Pb corrected in situ U-Pb accessory mineral geochronology by LA-MC-ICP-MS. The Royal Society of Chemistry, 18, 837–846. https://doi.org/10.1039/b304365g

Jackson, S. E., Pearson, N. J., Griffin, W. L., & Belousova, E. A. (2004). The application of laser ablation-inductively coupled plasma-mass spectrometry to in situ U-Pb zircon geochronology. Chemical Geology, 211(1–2), 47–69. https://doi.org/10.1016/j.chemgeo.2004.06.017

Palin, R. M., Searle, M. P., Waters, D. J., Parrish, R. R., Roberts, N. M. W., Horstwood, M. S. A., . . . Anh, T. T. (2013). A geochronological and petrological study of anatectic paragneiss and associated granite dykes from the Day Nui Con Voi metamorphic core complex, North Vietnam: Constraints on the timing of metamorphism within the Red River shear zone. Journal of Metamorphic Geology, 31(4), 359–387. https://doi.org/10.1111/jmg.12025

Rudnick, R. L., & Gao, S. (2003). 3.01 - Composition of the Continental Crust. In H. D. Holland & K. K. Turekian (Eds.), Treatise on Geochemistry (pp. 1–64). Oxford: Pergamon. https://doi.org/10.1016/B0-08-043751-6/03016-4

Slama, J., Kosler, J., Condon, D. J., Crowley, J. L., Gerdes, A., Hanchar, J. M., . . . Whitehouse, M. J (2008). Plesovice zircon — A new natural reference material for U-Pb and Hf isotopic microanalysis. Chemical Geology, 249(1–2), 1–35. https://doi.org/10.29 1016/j.chemgeo.2007.11.005

Stüwe, K. (1995). Thermal buffering effects at the solidus. Implications for the equilibration of partially melted metamorphic rocks. Tectonophysics, 248(1–2), 39–51. https://doi.org/10.1016/0040-1951(94)00282-E

Tomascak, P. B., Krogstad, E. J., & Walker, R. J. (1996). U-Pb monazite geochronology of granitic rocks from Maine: Implications for Late paleozoic tectonics in the Northern Appalachians. The Journal of Geology, 104, 185–195. https://doi.org/10.1086/629813

Wiedenbeck, M., Alle, P., Corfu, F., Griffin, W. L., Meier, M., Oberli, F., . . . Spiegel, W. (1995). Three natural zircon standards for U-Th-Pb, Lu-Hf, trace-element and REE analyses. Geostandards and Geoanalytical Research, 19(1), 1–23. https://doi.org/10.1111/j.1751-908X.1995.tb00147.x

Xu, Y., Shankland, T. J., Linhardt, S., Rubie, D. C., Langenhorst, F., & Klasinski, K. (2004). Thermal diffusivity and conductivity of olivine, wadsleyite and ringwoodite to 20 GPa and 1373 K. Physics of the Earth and Planetary Interiors, 143(1–2), 321–336. https://doi.org/10.1016/j.pepi.2004.03.005